

# Cemented paste backfill strength profiles for continuous pouring and liquefaction resistance

MW Grabinsky *University of Toronto, Canada*

BD Thompson *Paterson and Cooke, Canada*

RL Veenstra *Newmont, Australia*

## Abstract

*Current practice for backfilling tall stopes (e.g., long hole or Alimak) with cemented paste backfill (CPB) involves an initial plug pour to protect the barricade, followed by a main pour for the remaining stope. Many mines use higher binder content in the plug to accelerate curing time, supporting continuous pouring (i.e., no plug cure time before starting the main pour). An analytical solution to assess the required plug strength for continuous pours was recently proposed in a paper by Grabinsky et al. (2021). Similarly, various heuristics have been published suggesting a minimum Unconfined Compressive Strength will be sufficient to prevent CPB liquefaction under even the most implausible extreme loading events. However, practising mining engineers would benefit from a more straightforward design approach to assess the suitability of their backfill's evolving strength in continuous pour and liquefaction resistance design issues. To this end, the authors have found it useful to consider the concept of a Strength Profile with depth in the plug, recognising that this Strength Profile is transient (i.e., changing with time) and must be considered for different critical stages of the plug pour and main pour. The Strength Profile design concept is explained in this paper and demonstrated using key case histories from mines where the backfill was previously monitored during continuous pouring and where the backfill materials were extensively characterised in the laboratory.*

**Keywords:** *cemented paste backfill, continuous filling, plug stability analysis, liquefaction resistance*

## 1 Introduction

Backfill is the only form of global ground support to resist host rock closures and the associated build-up of potentially dangerous stress concentrations on a mine-wide scale. Of the three most common backfill forms, i.e., cemented paste backfill (CPB), cemented hydraulic fill (CHF), and cemented rock fill (CRF), CPB is currently preferred owing to its relatively fast delivery rate, the potential to tight fill the stope, and the opportunity to reuse the mine's generated tailings to the greatest extent possible, which then reduces the volume of waste materials reporting to surface disposal sites. CPB's Unconfined Compressive Strength (UCS) in the range of  $10^2$  to  $10^3$  kPa have been reported, with the highest UCS being about 5 MPa for Lucky Friday Mine and 6 MPa for Kidd Mine (which blends paste with esker sand to achieve higher densities) (Grabinsky et al. 2022). The opposite extreme timeframe from a design perspective occurs when the fresh CPB is deposited into the stope. For tall stopes (e.g., 100 m to 200 m high Alimak stopes), the theoretical fluid pressures exerted on the undercut's fill containment barricade could exceed 1 MPa if the fill remains fluid and in an undrained state. If the stope's bottom surface is free draining and stope arching effects are ignored, then Gibson's solution for accreting sediments (Gibson 1958) provides a basis for evaluating potential pore water pressure dissipation, as shown by Fahey et al. (2010) for idealised 'fast draining' and 'slow draining' stope conditions. However, most field instrumentation studies reported in the literature (Helinski et al. 2007; Thompson et al. 2011, 2012; Alcott et al. 2019) indicate that effective stress remains low in the backfill plug (i.e., less than 15 kPa effective stress) throughout the plug pour and into the main pour. Even when effective stresses appear, their development rates are typically below 5 kPa/h.

Geomechanical backfill design issues include the engineering of barricades, filling strategies, time to proximate blasting, sidewall exposure, undercutting, mining through fill, working on top of fill, and

liquefaction resistance. A common and largely unacknowledged design issue was that barricades commonly assume design loads consisting of the fluid plug height, relying on the plug (of height a few metres above the barricade) curing to isolate the barricade from the pressures induced by pouring the ‘main’ stope volume. However, to our knowledge, a formal definition of plug strength that would be adequate to isolate the barricade was lacking in the published literature. In response, Grabinsky et al. (2021) proposed a solution to determine the required strength for a backfill plug used in a continuously poured plug/main backfill filling strategy, where the plug is a higher binder content backfill poured to a few metres above the stope undercut’s brow, as seen in Figure 1.

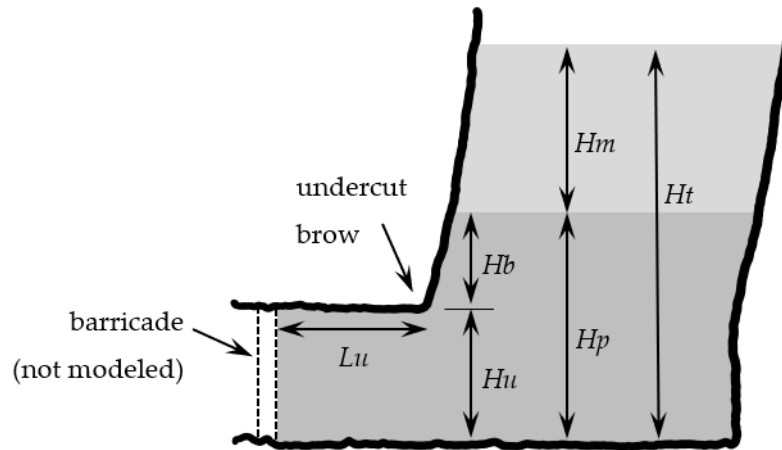


**Figure 1** Idealised plug and main pour geometry for a tall, backfilled stope.  $H_u$  and  $L_u$  are the height and length of the undercut, respectively;  $H_b$  is the height of backfill above the brow, and  $H_p$  is the total height of the plug;  $H_m$  is the (instantaneous) height of the main pour and  $H_t$  is the (instantaneous) total backfill height

However, the authors of Grabinsky et al. (op cit.) received feedback from consultants and mining personnel that the suggested design method (which uses the plug strength solution) is too general and onerous to implement, especially for preliminary design purposes. Therefore, our paper aims to present a simplified design approach for continuous pour analyses. Furthermore, continuously pouring the plug and main fills arguably offers the most likely opportunity for backfill liquefaction to occur in the context of placement of relatively large volumes of early-age backfill. Therefore, we make recommendations for combining the continuous pour analysis with a liquefaction risk assessment. As will be demonstrated with examples, utilising the concept of ‘strength profiles’, i.e., the backfill strength with depth in the backfill and with curing time, helps address both continuous pour and liquefaction design concerns.

We begin with a review of the background and design assumptions underlying the continuous pour analysis and then suggest how to implement the analysis technique in a simplified two-point design method using, in part, strength profiles. The liquefaction design concern is then addressed, and suggestions are made for risk assessment and mitigation. Finally, the ongoing design challenges associated with determining backfill strengths in the timeframes of continuous pours are reviewed.

## 2 Review of the Grabinsky et al. (2021) continuous pour analysis

Prior to the Grabinsky et al. (2021) plug strength analysis and design approach, there was limited reference to plug strength within the literature. To our knowledge, the only guidance was contained in the *Handbook on Minefill*, which stated that the plug should be poured to “...approximately 1 m above the draw point brow and permitted to cure to approximately 150 kPa strength before filling the remainder of the stope” (Potvin et al. 2005). Presumably, the “strength” is the Unconfined Compressive Strength (UCS) and the location where  $UCS = 150 \text{ kPa}$  would be at the top of the plug, although this was implicit. The referenced 1 m plug height above the brow may be considered inadequate as some operations likely cannot predict backfill height to

this level of accuracy. In our experience, several mines placed backfill plugs based purely on external strength requirements (i.e., vertical or undercut long-term strength) and paused backfilling by a period between 24 hours and seven days (in some cases, depending on risk exposure) before resuming the ‘main’ backfill pour. Some mines may never have formally defined a plug strength requirement, which is problematic if this plug strength was an implicit barricade design assumption. Others have assumed a plug strength requirement equivalent to the backfill’s unit weight  $\times$  height of the main pour. It should be acknowledged, therefore, that in the current environment where continuous backfilling is frequently discussed, a more formal need to define plug strength is required.

A rational engineered approach to plug strength design requires anticipating the potential failure mechanism, assessing the effective stress paths relevant to that mechanism, specifying the material strength under those stress paths, and determining the equilibrium condition, whether by Limit Equilibrium or continuum analyses, between the applied loads and the backfill resistance. Unfortunately, where barricades have failed, the failure surface in the backfill before the failure cannot be assessed because the subsequent rush of backfill erodes the surrounding backfill. Therefore, to investigate the failure mechanism using numerical analysis, it is necessary to know the total and effective stress states in the backfill at the time of failure.

## 2.1 States of stress in plug and main backfills during continuous pours

Fahey et al. (2010) considered the Gibson solution (Gibson 1958) for accreting sediments as the basis for evaluating the backfill’s pore water pressure dissipation and hence the development of effective stresses. The form of Gibson solution used assumes the stope’s bottom surface can freely drain away any water coming from the backfill’s bottom layer, and the sediment accretion rate (or backfill rise rate,  $m$ ) is constant. The important material assumptions follow the conventional consolidation analysis for soils, namely: the solid particles and the water phase are incompressible; the pore space is saturated (i.e., no occluded air bubbles nor continuous air phase); and the consolidation coefficient ( $c_v$ ) is a constant, which implies the coefficient of hydraulic conductivity (or permeability,  $k$ ) and the solid skeleton’s stiffness ( $M$ ) are constant. Unfortunately, all these assumptions are somewhat violated in backfill, which will be considered shortly.

Because the accreting sediments pose a ‘moving boundary’ problem type, Gibson (op cit.) presented the solution in the form of a series of normalised plots with the vertical axis being the normalised elevation ( $z$ ) in the accreting layer concerning the instantaneous layer height ( $H$ ) and the horizontal axis being the normalised pore water pressure ( $u$ ) with respect to the maximum possible slurry pressure ( $\gamma H$ , where  $\gamma$  is the slurry unit weight) at the bottom layer as if that boundary were impermeable. The predicted pore water pressure curves with normalised depth are expressed in terms of a time factor,  $T = mH/c_v$ ; therefore, fast consolidating backfills with high  $c_v$  values result in lower  $T$  values and smaller pore water pressures. Lower rise rates similarly result in lower  $T$  values. Smaller fill heights  $H$  also result in lower  $T$  values. Figure 2 shows an example of a hypothetical backfill with  $m = 0.25$  m/h,  $c_v = 0.078$  m<sup>2</sup>/h, and fill heights  $H = 2.5, 5.0, 7.5,$  and  $10.0$  m. The corresponding  $T$  values (with increasing  $H$ ) and normalised curves, as in Figure 2(a), are 8, 16, 24, and 32, and the scaled curves for instantaneous height and maximum slurry base pressure are shown in Figure 2(b). Notably, i) the pore pressure distribution approaches the slurry pressure gradient near the top of the instantaneous backfill height, ii) the pore water pressure is always zero at the assumed free draining bottom surface, and iii) for the constant material property assumption, the location of the maximum pore water pressure relative to the instantaneous height moves lower with fill height, and therefore the overall pore water pressure curve moves closer to the idealised slurry pressure gradient.

While the Gibson solution is useful conceptually, the binder hydration results in significant changes to hydraulic conductivity and backfill stiffness that have a tangible impact on the backfill’s corresponding  $c_v$  in cemented backfills. Shahsavari et al. (2022) studied these changes in detail using Williams mine CPB, where the increase in material stiffness with hydration was more significant than the reduction in hydraulic conductivity. So the corresponding  $c_v$  increased, making the backfill consolidate faster. Furthermore, several field monitoring programs (e.g., Thompson et al. 2011, 2012) have reported significant rises in backfill temperature resulting from the exothermic binder reaction, accelerating the binder reaction rates. The extent to which these effects impact the applicability of the Gibson solution is demonstrated next.

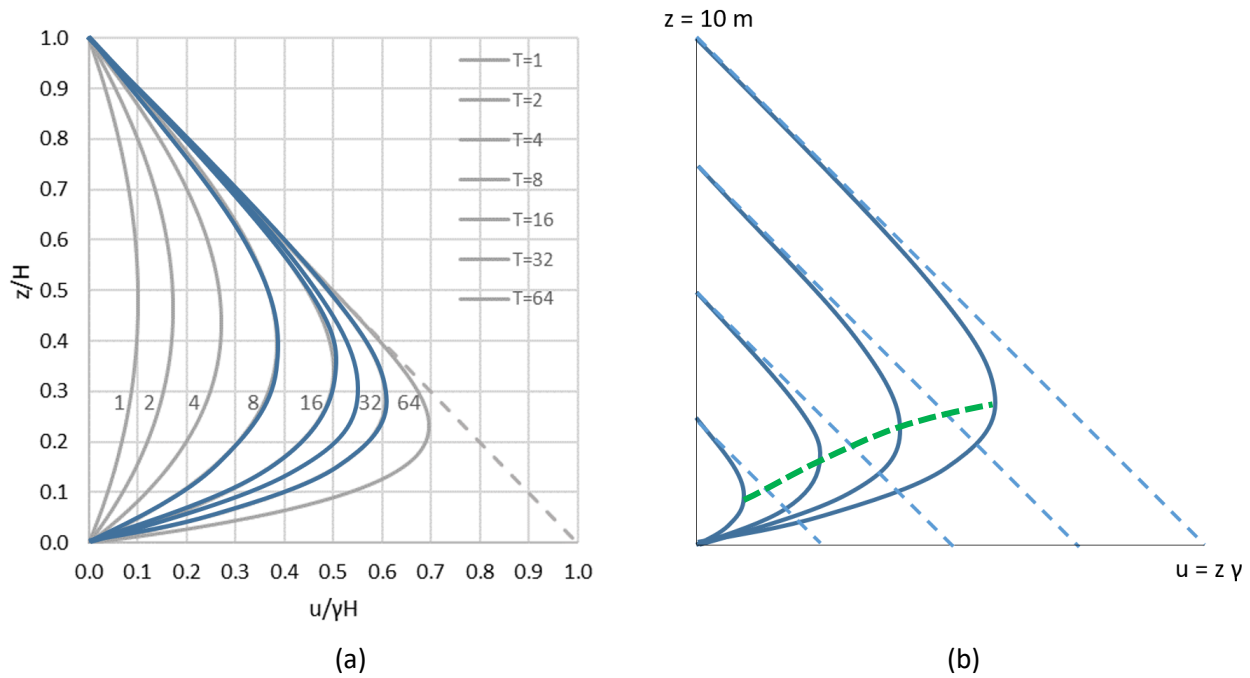


**Figure 2** Gibson solution for a hypothetical backfill deposition with rise rate 0.25 m/h,  $c_v = 0.078 \text{ m}^2/\text{h}$  and at instantaneous fill heights 2.5, 5.0, 7.5, and 10.0 m, in terms of (a) normalised values, and (b) actual values (Figure (b) shows the location of maximum pore water pressure with instantaneous height using broken green line)

## 2.2 Example states of stress in plug and main backfills from field monitoring

Figure 3 shows two stopes monitored at Kidd mine, referenced here as Stopes 67 and 88. Both were intended to be continuous pours with plug volumes containing approximately twice the binder content in the main pour to facilitate faster or higher strength gain. Stope 67 was poured continuously, aside from two minor interruptions in pouring.

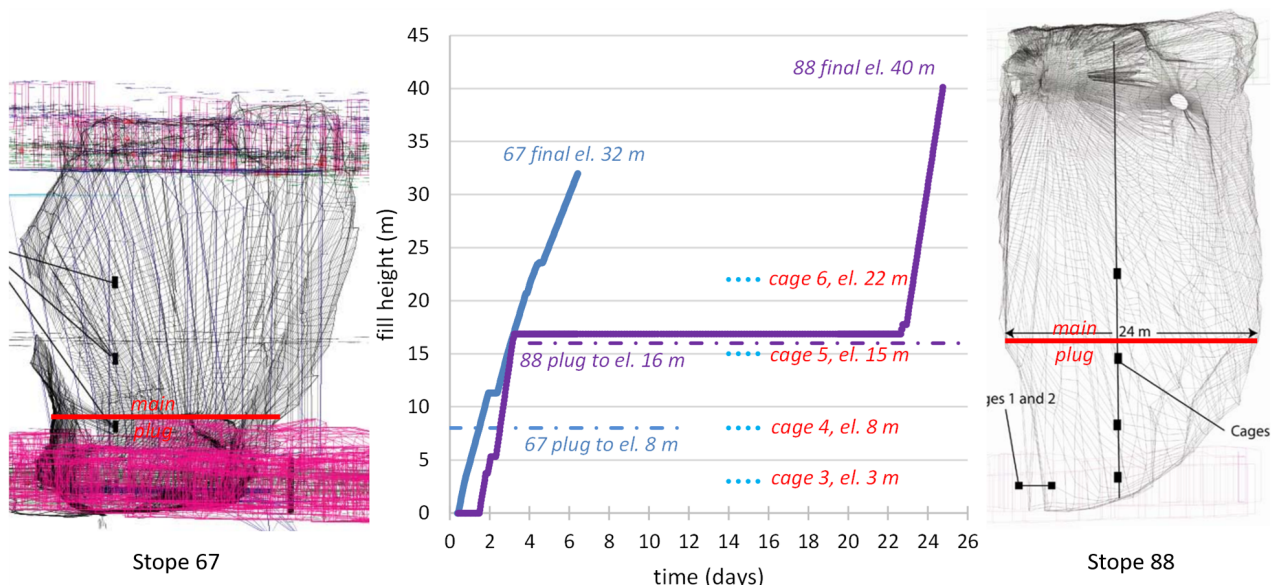


**Figure 3** Kidd mine monitored Stopes 67 and 88, showing geometry for 67 (left) and 88 (right), plug elevations, monitoring cage #s and elevations, and filling histories (centre)

Stope 88 poured to about 1 m above the plug height, and then operational factors caused a significant delay. However, a relatively large plug height of 16 m had been defined to enable subsequent undercutting. A 16 m

stope height is not unusual in the mining context, so useful information is provided by considering the 16 m height of continuous filling. The initial temperature in Stope 67 was about 23 °C while that in Stope 88 was 32 °C. The average rise rate in Stope 67 was about 0.3 m/h, while in Stope 88, it was about 0.5 m/h. Figure 4 shows measured pore water pressures with backfill height for Stope 67. It is evident that the main pour shows close to the theoretical slurry pressure gradients for unhydrated material for extended periods. However, the pressures in the plug quickly dissipate with hydration and remain virtually stagnant during the latter half of the pour. The pore water pressure at the bottom of the main pour near the plug/main interface does not fall to zero because the plug does not act as a free-draining boundary layer. However, it is unknown if the floor of the stope acts as a free-draining bottom layer for the plug because pore water pressure measurements cannot be made reliably at this interface, and the nature of the underlying material may be a variable in such analysis.

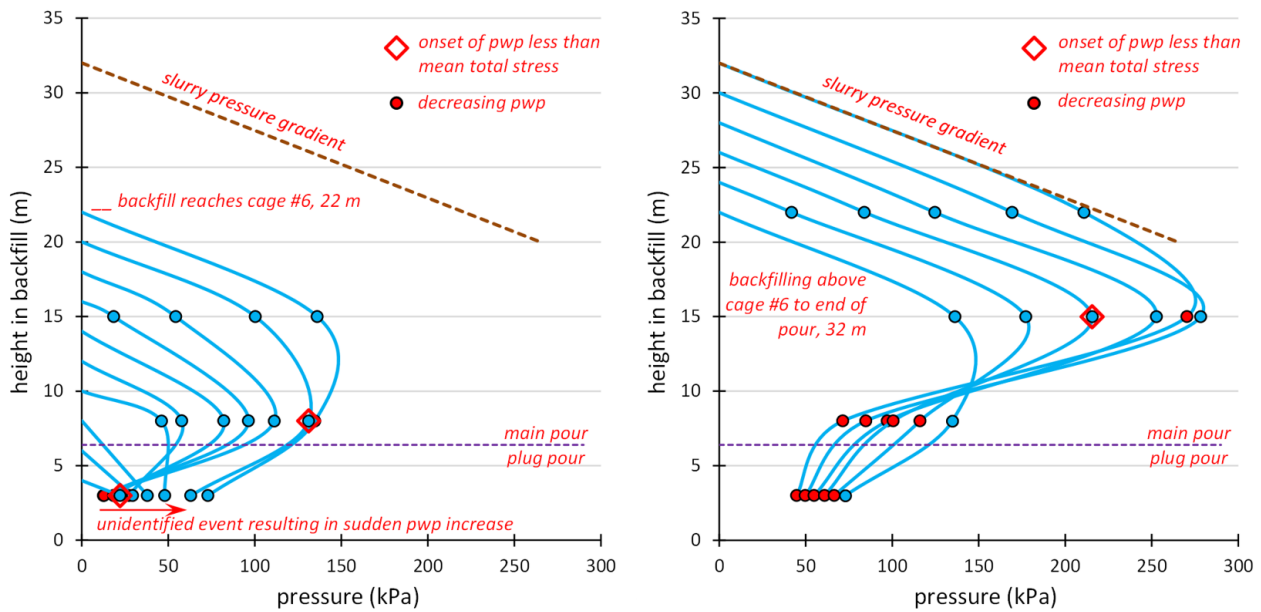


**Figure 4 Kidd Stope 67 pore pressure development with filling height for backfilling to 22 m height (left) and then to final height (right) (dot markers represent the locations of cage measurements)**

Stope 88 provides an interesting contrast, where the influence of curing temperature is noted in Figure 5. Early in Stope 88's filling history, the pore water dissipation is so extensive that the water pressure falls below the area's air pressure, resulting in 'suction' within the water phase. (The piezometers have porous plugs that begin desaturating at about 20 kPa suction, i.e., the Air Entry Value or AEV. Suctions up to 20 kPa are therefore considered reliable.) At the end of the plug pour, the maximum measured pore water pressure is about half that of Stope 67's for an equivalent height. This difference indicates the combined effects of binder content (i.e., Stope 67's plug has a thinner plug and therefore more 'main' backfill with lower binder content) and curing temperature (23 °C in Stope 67 versus 32 °C in Stope 88). Temperature differences could be attributed to seasonal differences in the ambient temperature of the backfill material (i.e., Spring versus Summer tests) and higher rock temperatures at the 8800 mine level. The combined results can better be compared using the Gibson normalised approach, shown in Figure 6. The lower binder content, main fill in Stope 67, when assessed as a single pour (dashed blue line), is consistent with a Gibson  $T = 16$  contour except near the bottom where the underlying plug does not provide a free-draining interface. If the entire Stope 67 is assessed (solid blue line), the influence of binder hydration in the plug can be seen where the pore water pressures are reduced significantly from the  $T = 16$  contour. Furthermore, assessing Stope 88 (purple line), where virtually the entire fill mass is higher binder content plug backfill, shows the dramatic reduction in pore water pressures to the extent that the lower approximately  $\frac{1}{4}$  of the plug is in suction at the end of backfilling.

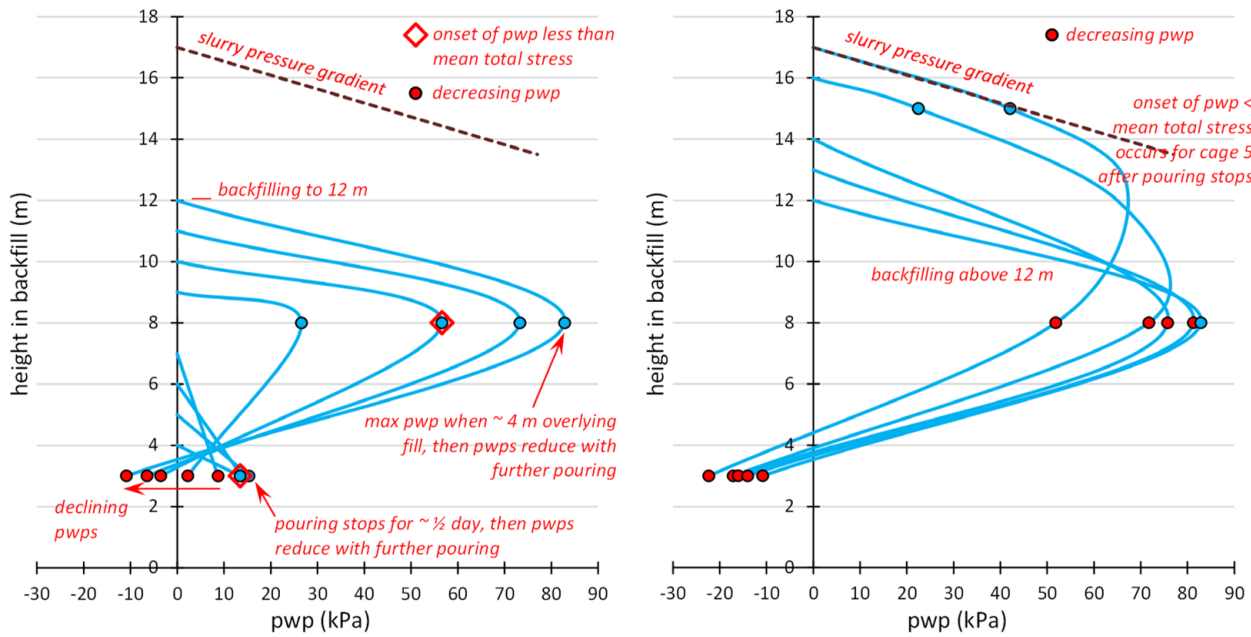


**Figure 5** Kidd Stope 88 pore pressure development with filling height for backfilling to 12 m height (left) and then to final height (right)

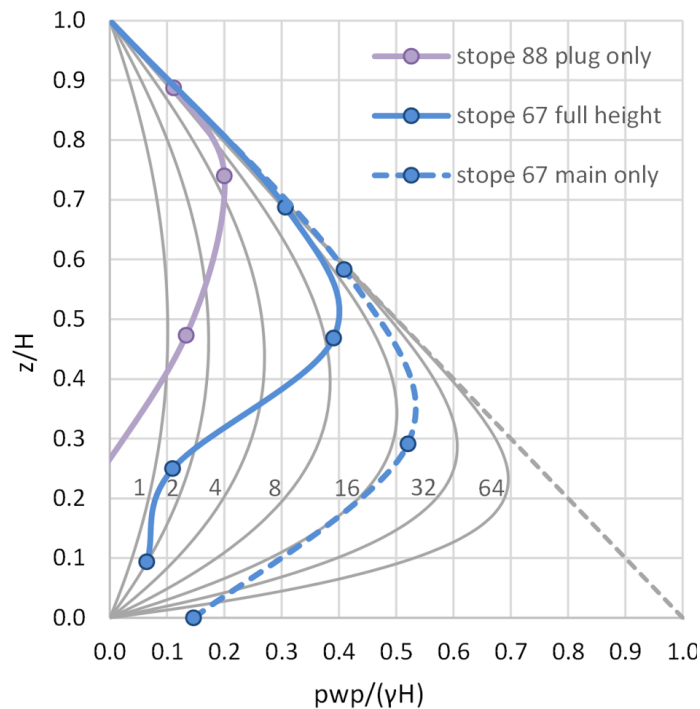


**Figure 6** Measured pore pressures at the end of filling for Kidd Stopes 67 and 88, compared using the Gibson approach.

Key conclusions are that lower binder content ‘main’ pours that hydrate slowly compared to the backfill rise rates (and hence, have larger T values) can result in essentially slurry pressure loading on the plug’s top surface, certainly when immediately transitioning during a continuous pour but possibly also well into the main pour. Secondly, the higher binder content plug pours will inevitably have lower T values than the corresponding main pours, especially if curing temperatures are elevated. From a stress analysis perspective and for plug stability analysis, the main pour should be regarded as slurry pressure. Still, the plug should be assumed to be capable of developing strength and stiffness due to binder hydration, even if effective stresses



remain relatively low. Grabinsky et al. (2021) provide further field monitoring results at other mines and conclude that the plug should be assumed to behave in the undrained state with zero effective stress development, at least for preliminary analysis, and the plug stability solution is developed on that basis. If further site-specific field monitoring demonstrates consistent, effective stress development during the early stages of a plug pour, then the suggested plug stability solution will be overly conservative from a safety perspective. The plug stability analysis based on these material and stress assumptions is given next.

### 2.3 Plug stability numerical analysis

Figure 7 shows a sample result from numerical analysis of plug stability based on the assumption that 1) the plug has only cohesive strength and responds in the undrained state (i.e., no effective stresses and no frictional strength component), 2) the main backfill pressure on the plug's top surface (shown as  $q$  in Figure 7b) is equal to the backfill unit weight  $\times$  instantaneous height of the main pour ( $Hm$  in Figure 1). Note that the numerical analysis 'finds' its failure mechanism, i.e., no artificial construct in the model generates a 'desired' failure mechanism.

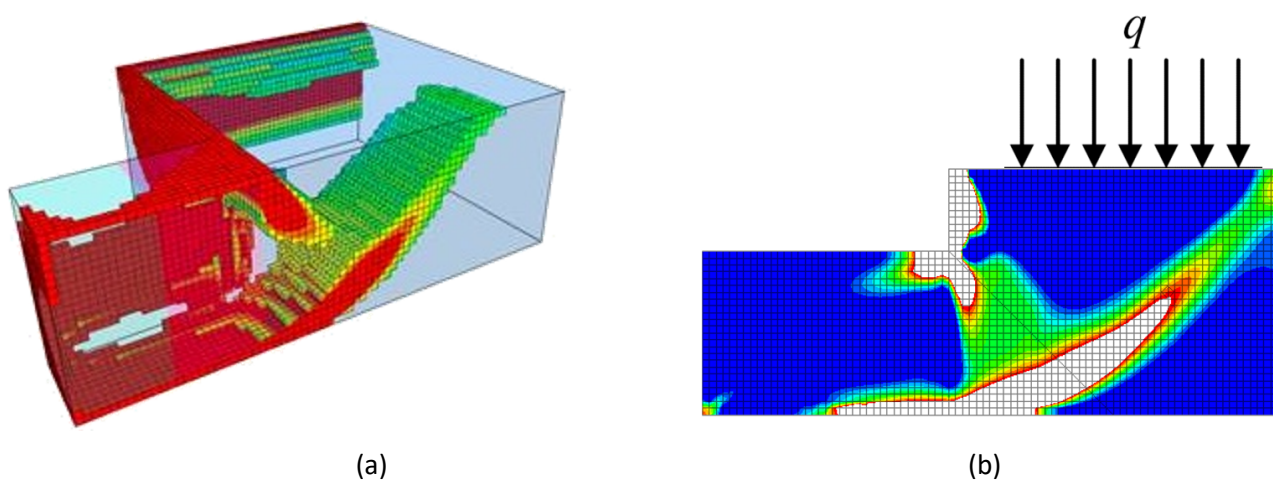


**Figure 7 Sample plug stability analysis showing plastic shear strain and development of failure surface in 3D (a) and 2D on the symmetry plane (b)**

Figure 7b shows shear failure generating on an inclined failure plane from the stope's wall opposite the undercut, then sweeping through an arc into the floor of the undercut. This failure shape is analogous to the  $\frac{1}{2}$ -mechanism formed under the edge of strip footing as assumed in the Prandtl solution and modified by Skempton (1951) for strip and spread footings on undrained clays. In this case, the stope's wall opposite the undercut must be at least  $1.5 H_u$  away (where  $H_u$  is the undercut height, Figure 1) for the failure mechanism to fully develop. If the stope is narrower than the drift (which may be true for Alimak stopes, for example), then the analysis will under-predict the actual plug stability. Furthermore, Figure 7a shows that the lateral extent of the failure mechanism is limited by the proximity of the undercut's sidewalls. Therefore, the actual stope width beyond the undercut width is not relevant. The geometric constraints of the failure mechanism should be considered for individual stope geometries and potential application of the plug stability analysis.

### 2.4 Calibrated analytical solution

The Skempton (1951) solution was used to motivate a particular solution to the plug stability analysis. This was then compared with numerical stability analysis results for a range of geometric parameters illustrated in Figure 1. The final form of the stability analysis is given in Equation 1,

$$\gamma(Hm + Hb + 0.55H_u) = c \left( 4 \frac{Hb}{H_u} + 3 + 4 \frac{Lu}{H_u} \right) \quad (1)$$

where the geometric terms are shown in Figure 1, and  $c$  is the materials cohesion. Equation 1 can be interpreted as follows: The left-hand side terms are the driving effects, including the pressure arising from

the main pour ( $\gamma H_m$ ), the pressure from the portion of the plug above the brow ( $\gamma H_b$ ), and the equivalent stress arising from the self-weight of the Prandtl  $\frac{1}{2}$ -mechanism ( $\gamma 0.55 H_u$ ; note that the factor 0.55 was empirically derived from numerical analysis). Note that the self-weight of the plug portion in the undercut between the brow and the barricade does not contribute to the driving mechanisms. The terms on the right-hand side are the resisting effects, including material resistance to shearing through the plug portion above the brow ( $4c H_b/H_u$ ), to shearing through the Prandtl  $\frac{1}{2}$ -mechanism ( $3c$ ), and to shearing around the perimeter of the portion of the plug in the undercut ( $4c L_u/H_u$ ).

## 2.5 Selection of material strength

The strength parameter in Equation 1 is cohesion,  $c$ , because the analysis assumes zero effective stress, so only relying on cohesion. The relationship between drained strengths obtained from UCS, direct shear, and direct tension tests was investigated by Pan (2019) and is shown in Figure 8 for a particular binder content and cure time. The results are generally consistent and indicate that cohesion can reasonably be correlated to UCS, which is useful because UCS is the most used type of strength assessment. For typical drained friction angles (i.e.,  $27^\circ$  to  $36^\circ$ ), the correlation is generally  $c = 0.25UCS$  to  $0.30UCS$ . Therefore, in the absence of specific test data to provide the friction angle, it is conservative (from a safety perspective) to assume  $c = \frac{1}{4}UCS$ .

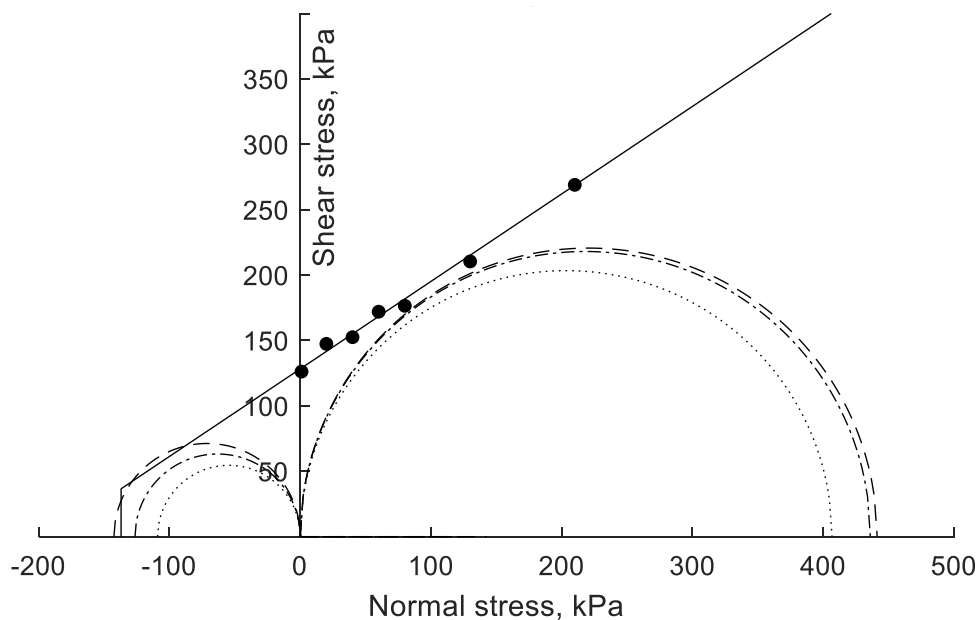


**Figure 8 Relationship between drained strengths obtained from UCS, direct shear, and direct tension tests**

## 2.6 Influence of variable material strength

At the end of the plug pour, the initially poured backfill near the bottom of the stope will have cured for many hours and gained tangible strength and stiffness, while the backfill at the plug's top surface is still in a slurry state. To assess the influence of such variable strength, the constant strength analyses from Section 2.3 (above) were compared with linearly varying strength models, with the constraint that the strength at the mid-height of the undercut is the same as used in the constant strength model. These models give similar ultimate pressures to failure, indicating it is appropriate to use the pour time when the backfill reaches the undercut's mid-height as the time zero for assessing strength development with hydration (i.e., from the perspective of laboratory validation, samples should be taken equivalent to the undercut mid-height).

## 3 Simplified 'two-point' design

Compared to the originally proposed design approach by Grabinsky et al. (2021), several simplifying assumptions are appropriate, especially for preliminary design. This simplified approach is particularly



amenable to spreadsheets, and such implementation will be illustrated in this section. With reference to Figure 1, it is assumed that the main stope is vertical and the backfill volume delivery rate is constant so that only the rise rate in the undercut area below the brow ( $r_{ru}$ ) and the rise rate in the main stope above the brow ( $r_{rm}$ ) need to be considered. All input for the required strength analysis is shown in Figure 9. As indicated in Section 2.6, it is important to differentiate the ‘time since the start of pouring’ from the ‘reference cure time’, which starts when the backfill reaches the undercut’s mid-height. Therefore, also shown in Figure 9 are the three relevant times, 1) the time to reach the undercut’s mid-height ( $t_{ref}$ ), which is then the time zero with respect to backfill curing; 2) the time in addition to  $t_{ref}$  required to finish the plug pour, ( $t_{plug}$ ), which is now the reference curing time for the plug, and 3) the time in addition to  $t_{ref}$  required to complete backfilling ( $t_{end}$ ). These are computed using Equations 2a,b,c,

$$t_{ref} = (H_u/2)/r_{ru} \quad (2a)$$

$$t_{plug} = (H_u/2)/r_{ru} + H_b/r_{rm} \quad (2b)$$

$$t_{end} = t_{plug} + H_m/r_{rm} \quad (2c)$$

Simplified Continuous Pour Analysis			
<b>Required Input</b>			
Backfill unit weight	gamma	21.5	kN/m <sup>3</sup>
Height of undercut	H <sub>u</sub>	5	m
Length of undercut	L <sub>u</sub>	12	m
Height above brow	H <sub>b</sub>	2	m
Height of main pour	H <sub>m</sub>	23	m
fill rise rate in undercut	r <sub>ru</sub>	0.1667	m/h
fill rise rate above brow	r <sub>rm</sub>	0.2	m/h
<b>Calculations</b>			
time to H <sub>u</sub> /2	t <sub>ref</sub>	14.997	h
(time to reach H <sub>p</sub> ) - t <sub>ref</sub>	t <sub>plug</sub>	24.997	h
(time to end of filling) - t <sub>ref</sub>	t <sub>end</sub>	139.997	h

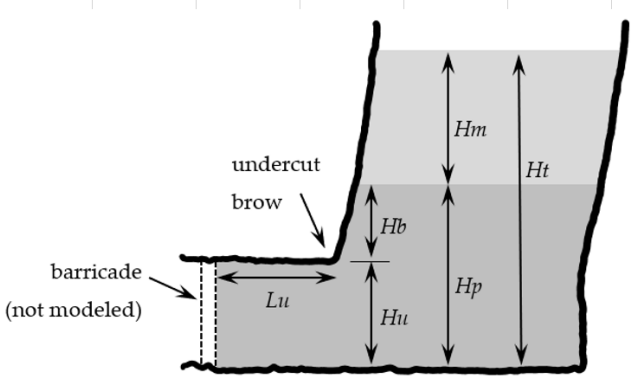


**Figure 9** Input screenshot for required plug strength analysis

### 3.1 First point: self-supporting plug strength

The limiting cohesive strength (i.e., for Strength Factor = 1) for the plug at the end of pouring can be calculated using Equation 1 with  $H_m = 0$  and normalised as shown in Equation 3,

$$\frac{c_{ss}}{\gamma H_u} = \frac{0.55 + H_b/H_u}{3 + 4H_b/H_u + 4L_u/H_u} \quad (3)$$

where  $c_{ss}$  is the self-supporting cohesion, such that the plug would remain stable under its self-weight even if the barricade were removed (although removing the barricade at this point is extremely imprudent). Equation 3 is expressed in normalised form to facilitate comparisons between case histories, as shown in Figure 10. Note that for undercut height  $H_u = 5$  m and backfill unit weight  $\gamma = 20$  kN/m<sup>3</sup>, and using the previous assumption  $UCS = 4c$ , the vertical axis is scaled by a factor 100 to get UCS<sub>ss</sub> in kPa, where UCS<sub>ss</sub> is the equivalent self-supporting UCS. In this case, the range of limiting UCS values (i.e., SF = 1.0) is from approximately 20 kPa for significant setbacks ( $L_u/H_u$ ) and modest pour heights above the brow ( $H_b/H_u$ ) to about 75 kPa for minor setbacks and considerable pour heights above the brow. Even applying reasonable strength factors to these limiting values results in UCS values much less than the empirically suggested 150 kPa. Furthermore, Figure 10 makes assessing the significance of the setback distance  $L_u$  and the pour height above the brow  $H_b$  easy, allowing engineers to conduct site-specific cost-benefit assessments on these parameters.

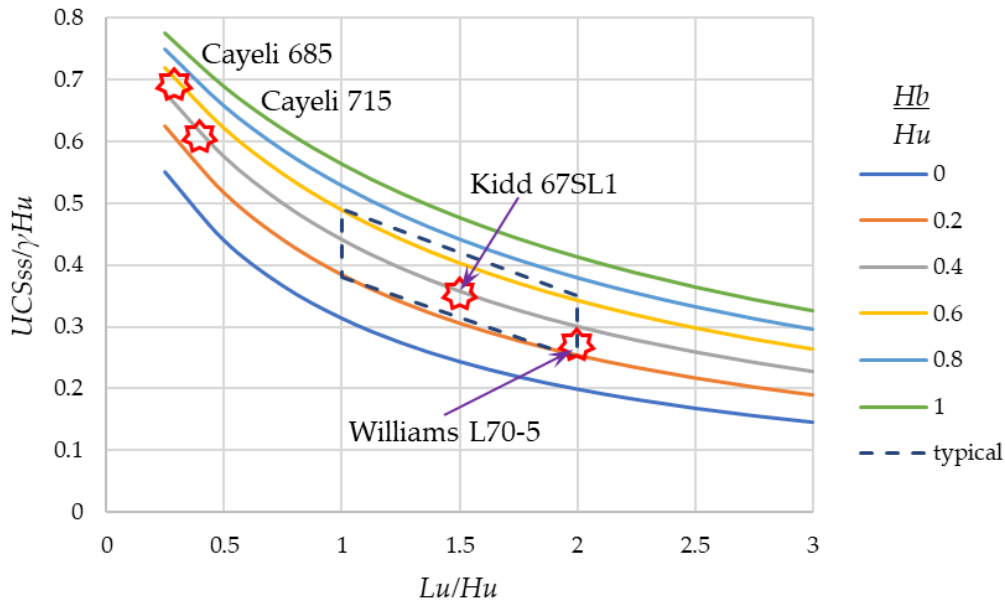


**Figure 10 Self-supporting plug cohesion for case histories used in the continuous pour analysis**

### 3.2 Second point: plug strength at the end of the main stope pour

Equation 1 shows that the required plug cohesive strength increases linearly with the main pour height ( $H_m$ ). Setting  $H_m = 0$  results in the self-supporting condition described in the previous section. If the rise rate in the main pour is constant at  $r_{rm}$  as assumed, then the corresponding required cohesion also increases at a constant rate, i.e., increases linearly with time. Therefore, it is only necessary to compute the required cohesion at the end of pouring ( $c_{end}$ ), using Equation 4,

$$\frac{c_{end}}{\gamma H_u} = \frac{c_{ss}}{\gamma H_u} + \frac{H_m/H_u}{3 + 4H_b/H_u + 4Lu/H_u} \quad (4)$$

### 3.3 Comparisons with strength gains

Using the input data shown in Figure 9, the computed cohesion values (for  $SF = 1.0$ ) are  $c_{ss} = 7.2$  kPa and  $c_{end} = 42$  kPa, or approximately  $UCS_{ss} = 30$  kPa and  $UCS_{end} = 170$  kPa. The corresponding cure times are  $t_{plug} = 25$  h and  $t_{end} = 140$  h (or just under six days). Note that achieving quality UCS results at such low strengths requires great care in testing, discussed in the final section. Figure 11 shows cohesive strength gains of CPB with cure time for three different binder contents (for an unspecified mine). Recall that the cure time is referenced concerning when the backfill reached the undercut’s mid-height. Therefore, the value  $t_{ref}$  must be added to these values to get the equivalent pour time. Considering when the plug finishes pouring in Figure 11, indicated as ‘main pour start’, 3.0% binder content is insufficient, 5.3% binder content is marginally sufficient, and 7.5% binder content provides a strong Strength Factor (approximately 3.5 times greater cohesion available than is required for the plug to be self-supporting). For the marginal case of binder content of 5.3%, the available cohesion is only exceeded by the theoretical strength requirement near the end of the pour. However, in most cases, effective stresses will have developed in the plug by then, so a continuous pour at 5.3% for the considered backfill is plausible, if not conservative. For the strongest case of binder content of 7.5%, the available Strength Factor gradually reduces during the pour; in theory, at the end of the pour, it is about 1.75. But, in this case, it is even more likely that effective stresses will have developed in the plug owing to the higher binder content and likely greater heat generation resulting in acceleration of strength gains.

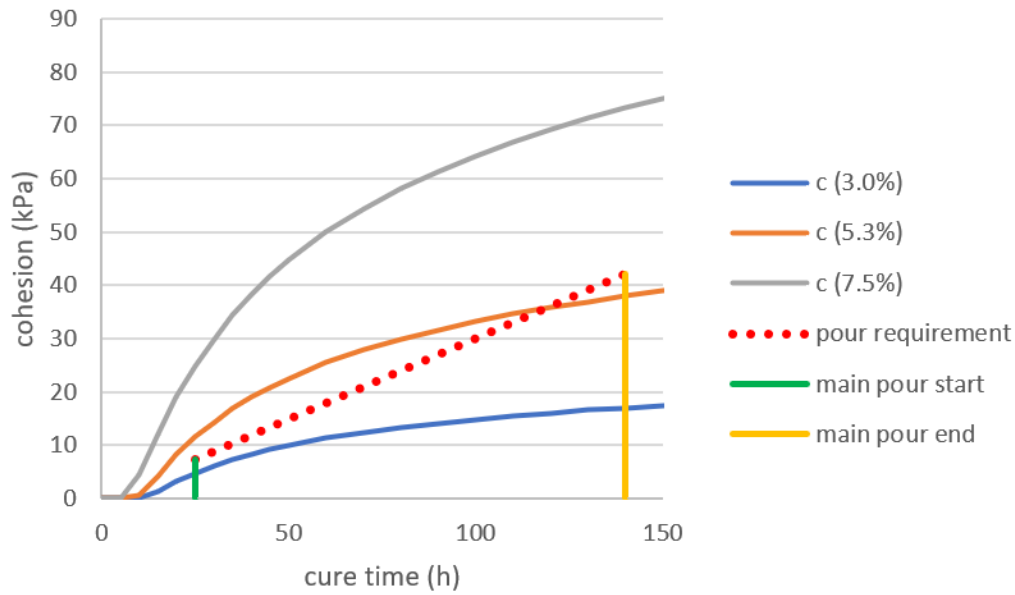


**Figure 11 Comparing limiting UCS requirements ( $SF = 1.0$ ) with UCS test data for three binder contents**

### 3.4 Visualising strength gains with depth and time using strength profiles

In the above analysis, the strength gain with cure time is focussed on one position, i.e., at the undercut's mid-height. However, the strength will continuously evolve throughout the plug height, and it is useful to visualise how this will take place. Recall in the example used here that the curing time to finish the plug is  $t_{\text{plug}} = 25$  h and that the backfill rise rate in the main stope is  $r_{\text{rm}} = 0.2$  m/h, or 5 m every 25 h. In this case, the 'curing time' on the horizontal axis in Figure 11 can be converted to an equivalent depth axis with every 25 h representing 5 m depth and with the origin corresponding to the instantaneous height of the main backfill. This is illustrated in Figure 12.

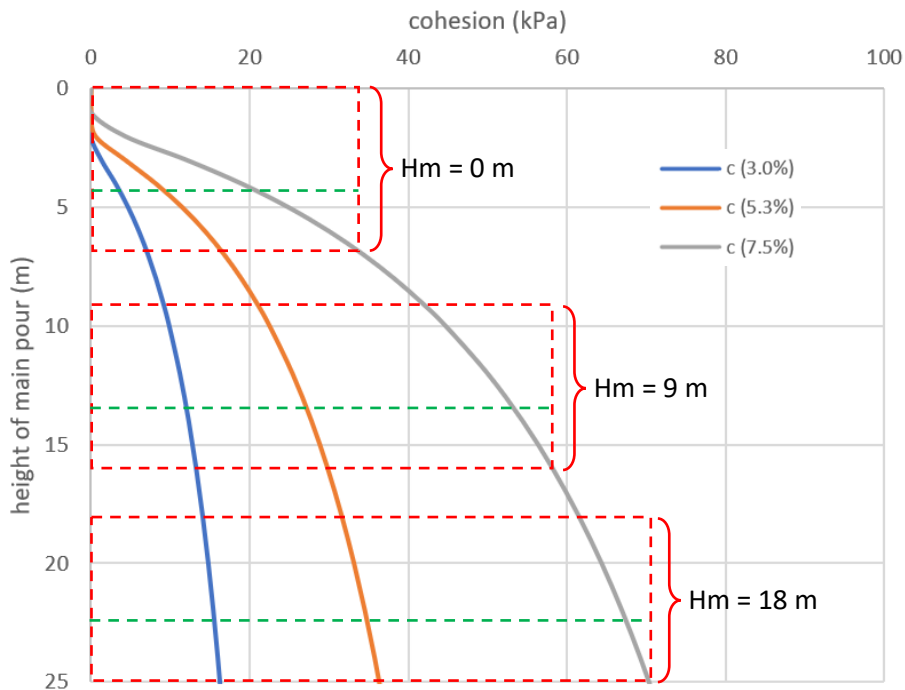


**Figure 12 Strength profiles with plug depth at main pour heights  $H_m = 0, 9,$  and  $18$  m (dashed red lines indicate the top and bottom of the plug, and the green dashed line indicates the undercut's mid-height).**

The dashed red lines indicate the full plug height (7 m), and the dashed green line represents the undercut’s mid-height, but the strengths below the reference green line are approximate because of the variation in the rise rate. The approximation is appropriate for the intended visualisation purpose. As should be expected, the strength variations for the sample CPB are most extreme immediately upon plug completion ( $H_m = 0$ ), and the strengths become increasingly uniform with depth at later curing times and corresponding main pour heights. In Figure 12, an estimate is obtained of backfill depth that remains un-hydrated (i.e.,  $c = 0$ ) for the case of plug pour completion ( $H_m = 0$ ). This has implications for liquefaction assessment.

#### 4 Liquefaction assessment, mitigation, and preparedness

The plug strength method requires site-specific risk assessment, and liquefaction potential may be one such risk. The strength profile concept may be expanded to better define risks associated with liquefaction. Suazo et al. (2017) suggest that the 100 kPa commonly cited minimum UCS for liquefaction resistance of CPB is likely conservative. These authors note that the liquefaction risk should not be overstated, especially when assessing the likelihood of significant earthquake-type loading events. While questions remain on the effect of mine-related blasting near fresh CPB, liquefaction-related incidents regarding paste are not reported in the literature to our knowledge. Irrespective of liquefaction risk, a minimum strength requirement for CPB is sensible under most circumstances to eliminate the potential energy source that a large volume of fluid CPB represents.

The Kidd Stope 67 is a valuable case study where two significant production blasts occurred in an adjacent stope at 131 and 144 days after pouring. This data is helpful on a fundamental level in defining dynamic loading events occurring at this specific site. Two cages in the lower binder content backfill volume (with UCS  $\sim 1$  MPa from core samples) had all three total pressure cells and piezometer functioning. Evaluating liquefaction potential in terms of a required UCS has been common. While this is convenient, it understates the complexity of liquefaction phenomena in structured (including cemented) materials. One way of assessing the liquefaction potential is to evaluate the pore pressure response to changes in mean stress (i.e., the average of the three total stress changes), which is termed the B-value during the back-pressure saturation phase of consolidated triaxial testing. A B-value of 1.0 indicates the water phase fully carries the changes in mean stress, and the pore space is saturated (no occluded air ‘bubbles’). In contrast, values less than 1.0 indicate decreasing saturation degrees and liquefaction potential. In triaxial testing for liquefaction assessments, a B-value of at least 0.97 is generally adequate for the test to be considered valid. The equivalent B-value analysis for one of the Kidd 67 cages is shown in Figure 13. The peak mean stress transfer to the water phase was only about 30% for both blasting events, indicating it would be challenging to liquefy this backfill because stresses are not effectively transmitted to the fluid phase.

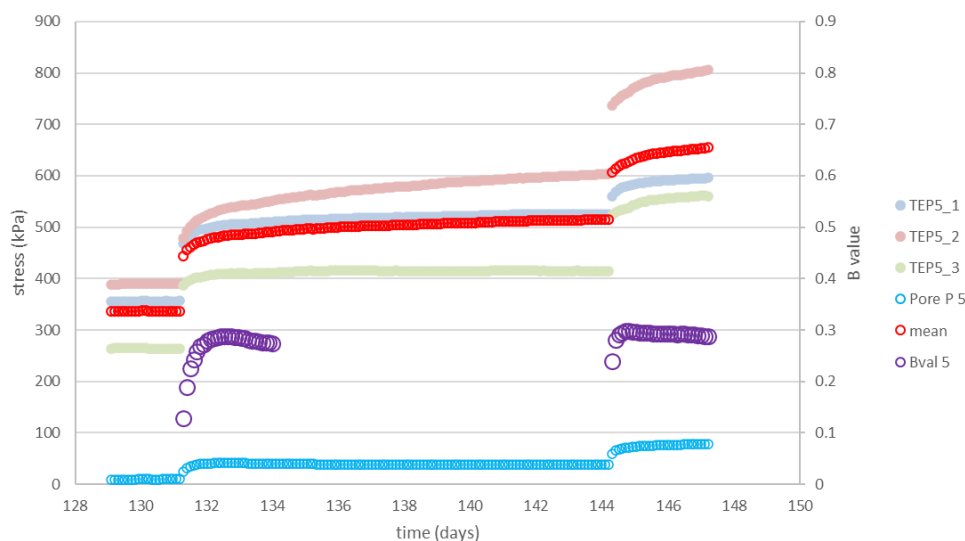


**Figure 13 B-value analysis for a monitoring cluster in the main backfill of Kidd 67, response to adjacent production blasting at days 131 and 144**

More significantly, a Mn 3.8 rockburst occurred 220 days after pouring 200 m from Stope 67. At least one transducer had previously stopped functioning in each main pour cluster, so B-value analysis cannot be carried out. However, Figure 14 shows the backfill's pore pressure profiles with depth for pre- and post-production blasting and rockburst events, and the overall effect of the rockburst was *less* than that of the production blast. The maximum water pressure readings at the uppermost cage correspond to a pore pressure gradient less than half of hydrostatic (i.e., as compared to hypothetical ponded water at the top surface of a backfill), again indicating a very low potential for liquefaction in this stope.

The data presented is anecdotal, and liquefaction would be implausible with UCS exceeding 1 MPa. More concern would exist for relatively early-age fills under similar loading conditions. When UCS is used as the 'liquefaction resistance' criterion, it should be considered site-specific. The strength profiles in Figure 12 show that there will be instances where CPB remains in a liquefied (slurry) state at the end of the plug pour. These profiles can then be used to assess the depth to which the plug's backfill may remain liquefied or persist below a UCS that would pose a theoretical risk of liquefaction.

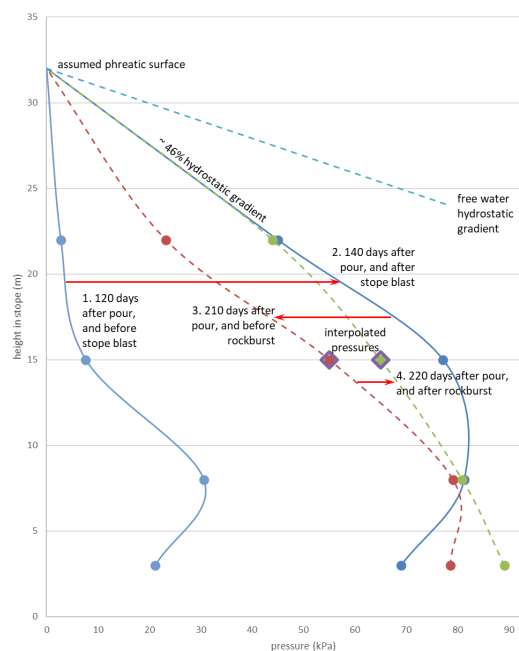


**Figure 14** Pore pressure profiles in response to blasting and rockburst events

#### 4.1 Liquefaction mitigation and preparedness

The plug stability analysis method assumes the main backfill volume remains slurry and exerts full fluid head pressure on the plug's upper surface. Inducing liquefaction of plug material below the brow's elevation would therefore breach assumptions in the calculation and could theoretically lead to the full pressure head bearing directly on the barricade. Potential mitigation measures include increasing the plug's binder content to achieve the specified strength at a safe elevation above the brow and ensuring adequate barricade design.

The risk of CPB outflow resulting from barricade failure, induced by liquefaction or other causes, can be mitigated using exclusion zones. Many mines employ such measures, assuming that containment berms will retain a fluid or potentially fluid volume of CPB. The Strength Profile analysis provides means to efficiently define the required volume by recognising when the strength of the upper layer of the plug exceeds all reasonable estimates for mobilising, which can include provision for liquefaction susceptibility.

## 5 Conclusion

We have suggested a simplified 'two-point' plug stability analysis method, focussing on backfill strength gains at the undercut's mid-height at the end of plug pouring and the backfilling sequence's end. This method is

particularly convenient for preliminary design but can be adapted to more general use if deemed appropriate by a given mine. It is also essential to consider the variation of strength within the backfill plug with depth and time. In this context, the demonstrated concept of ‘strength profiles’ are helpful, especially when considering the potential design issue of liquefaction.

Defining appropriate criteria for backfill liquefaction resistance remains elusive. But, if an equivalent cohesive strength or UCS is selected, then the strength profiles can be used to assess liquefaction potential during pouring and develop mitigation measures to contain potentially liquefied backfill and prepare emergency plans should a liquefaction event breach the containment barricade.

Generally, this approach requires careful QA/QC processes, and Grabinsky et al. (2022) have reviewed the early-age strength assessment of CPB. It should also be emphasised that this method is an analytical framework to define adequate CPB early-age strength for safe backfilling, calibrated using fieldwork data. We anticipate that, in time, additional field data verification will be provided as mines apply the proposed approach. However, we also advise caution and independent verification using instrumentation to ensure safe loading conditions at barricades is a minimum requirement to ensure safe backfilling. Site-specific assessments are always recommended.

## Acknowledgement

The continuous pour analysis and liquefaction risk assessment methods were developed from extensive field and laboratory work carried out under several research project phases named Geomechanical Design of Cemented Paste Backfill Systems, supported by Williams, Kidd, and Cayeli mines (and their respective corporate owners at the time, namely Barrick Gold, Xstrata/Glencore, and Inmet), and the Natural Sciences and Engineering Research Council Canada through Collaborative Research and Development (CRD) grants.

## References

- Alcott, J, Dallaire, D & Belem, T 2019, ‘Pastefill optimization at Hecla Quebec’s Casa Berardi mine’, in *Proceedings of the 53rd US Rock Mechanics/Geomechanics Symposium*, American Rock Mechanics Association, Alexandria, paper no. ARMA-2019-0231
- Fahey, M, Helinski, M & Fourie, A 2010, ‘Consolidation in accreting sediments: Gibson’s solution applied to backfilling of mine stopes’, *Géotechnique*, vol. 60, no. 11, pp. 877–882, <https://doi.org/10.1680/geot.9.P.078>
- Gibson, RE 1958, ‘The progress of consolidation in a clay layer increasing in thickness with time’, *Géotechnique*, vol. 8, no. 4, pp. 171–183, <https://doi.org/10.1680/geot.1958.8.4.171>
- Grabinsky, M, Jafari, M & Pan, A 2022, ‘Cemented Paste Backfill (CPB) material properties for undercut analysis’, *MDPI Mining Journal, Special Edition on Application of Empirical, Analytical, and Numerical Approaches in Mining Geomechanics*, vol. 2, no. 1, pp. 103–122, <https://doi.org/10.3390/mining2010007>
- Grabinsky, M, Thompson, B & Bawden, W 2021, ‘Required plug strength for continuously poured cemented paste backfill in longhole stopes’, *MDPI Mining Journal, Special Edition on Application of Empirical, Analytical, and Numerical Approaches in Mining Geomechanics*, vol. 1, no. 1, pp. 80–99, <https://doi.org/10.3390/mining1010006>
- Helinski, M, Fahey, M & Fourie, A 2007, ‘Numerical modeling of cemented mine backfill deposition’, *Journal of Geotechnical and Geoenvironmental Engineering*, vol. 133, pp. 1308–1319, [https://doi.org/10.1061/\(ASCE\)GT.1943-5606.0000418](https://doi.org/10.1061/(ASCE)GT.1943-5606.0000418)
- Pan, A 2019, *Mechanical Properties of Cemented Paste Backfill under Low Confining Stress*, Master’s Thesis, University of Toronto, Toronto, <http://hdl.handle.net/1807/98310>
- Potvin, Y, Thomas, E & Fourie, A 2005, *Handbook on Mine Fill*, Australian Centre for Geomechanics, Perth.
- Shahsavari, M, Jafari, M & Grabinsky, M 2022, ‘Influence of load path and effective stress on one-dimensional deformation of Cemented Paste Backfill (CPB) during deposition and curing’, *Geotechnical and Geological Engineering*, vol. 40, pp. 2319–2338, <https://doi.org/10.1007/s10706-021-02030-4>
- Suazo, G, Fourie, A & Doherty, J 2017, ‘Cyclic shear response of cemented paste backfill’, *Journal of Geotechnical and Geoenvironmental Engineering*, vol. 143, no. 1, article no. 04016082, [https://doi.org/10.1061/\(ASCE\)GT.1943-5606.0001581](https://doi.org/10.1061/(ASCE)GT.1943-5606.0001581)
- Skempton, AW 1951, ‘The bearing capacity of clays’, in *Proceedings of the Building Research Congress, London, England, 11-20 September 1951*, Institution of Civil Engineers, London, pp. 180–189. Reproduced by permission, National Research Council of Canada, <https://doi.org/10.4224/40000389>
- Thompson, B, Bawden, WF & Grabinsky, M 2012, ‘In situ measurements of cemented paste backfill at the Cayeli Mine’, *Canadian Geotechnical Journal*, vol. 49, pp. 755–772, [doi.org/10.1139/t2012-040@cgj-ec.2015.01.issue-1](https://doi.org/10.1139/t2012-040@cgj-ec.2015.01.issue-1)
- Thompson, B, Grabinsky, M & Bawden, W 2011, ‘In situ monitoring of cemented paste backfill pressure to increase backfilling efficiency’, *CIM Journal*, Canadian Institute of Mining, vol. 2, no. 4, pp. 199–209.